Technical Memo

ECMWF
European Centre for Medium-Range Weather Forecasts

869

Potential temperature as a prognostic variable in hydrostatic semi-implicit semi-Lagrangian IFS

Inna Polichtchouk, Sylvie Malardel and Michail Diamantakis

August 2020

Series: ECMWF Technical Memoranda

A full list of ECMWF Publications can be found on our web site under:
http://www.ecmwf.int/en/research/publications

Contact: library@ecmwf.int

European Centre for Medium-Range Weather Forecasts
Shinfield Park, Reading, RG2 9AX, England

Abstract

Thermodynamic equation in the operational ECMWF Integrated Forecasting System (IFS) dynamical core is formulated to use temperature as a prognostic variable. An alternative formulation, using potential temperature as a prognostic variable in hydrostatic semi-implicit semi-Lagrangian IFS, is investigated. Different from temperature, potential temperature is materially conserved in the absence of sources and sinks. The new equation set is first derived. Then the performance of free-running IFS (i.e., without data assimilation) using potential temperature as a prognostic variable is compared to the control formulation using temperature as a prognostic variable. It is shown that the potential temperature formulation performs comparably to the temperature formulation under several tests, ranging from adiabatic idealized test cases to medium-range weather forecasts with full physical parametrization suite.

1 Introduction

In the operational ECMWF IFS dynamical core, temperature is currently used as a prognostic thermodynamic variable. Here an alternative implementation using potential temperature as a prognostic variable in the hydrostatic semi-implicit semi-Lagrangian (SISL) IFS is investigated. In contrast to temperature, potential temperature is conserved in an adiabatic atmosphere. This property makes it a potentially more desirable thermodynamic variable for use in a numerical weather prediction (NWP) model. Therefore some NWP models, including the UK Met Office Unified Model (Wood et al., 2014) and US Navy's Navy Global Environmental Model (NAVGEM, Hogan et al., 2014) use potential temperature as a prognostic variable.

To what extend potential temperature formulation affects performance of the IFS is investigated in this report, which is structured as follows: In section 2, the hydrostatic primitive equations using potential temperature as a prognostic variable are given and the semi-implicit formulation is derived. Comparison of solutions with potential temperature as a prognostic variable (henceforth IFS-θ) to those with temperature as a prognostic variable (henceforth IFS-CTRL) are presented in section 3 for several idealized adiabatic test cases. In section 4, full-physics IFS solutions are compared for an ensemble of one year free-running forecasts, and for medium-range weather forecasts. Finally conclusions are given in section 5.

2 Hydrostatic primitive equations: potential temperature as a prognostic thermodynamic variable

Adiabatic SISL hydrostatic primitive equations using potential temperature (θ) in IFS are presented here. When changing variable from temperature (T) to potential temperature (θ), the thermodynamic, the momentum and the hydrostatic balance equations need to be reformulated in terms of $\theta = T(p_{00}/p)^{\kappa}$, where p is pressure, p_{00} =1000 hPa, and $\kappa = R_d/c_{pd}$ where R_d is the gas constant for dry air and c_{pd} is the specific heat of dry air at constant pressure. In η vertical coordinate (Simmons and Burridge, 1981), the momentum equation is:

$$\frac{D\mathbf{V}}{Dt} + f\mathbf{k}\times\mathbf{V} + \nabla_h\Phi + R_d\theta_v\left(\frac{p}{p_{00}}\right)^{\kappa}\nabla_h \ln p = 0, \tag{1}$$

where $\mathbf{V} = (U,V) = (u\cos\phi, v\cos\phi)$ and ϕ is latitude, f is the Coriolis parameter, ∇_h is the horizontal gradient operator on constant η-surfaces, Φ is the geopotential, θ_v is the virtual potential temperature

$$\theta_v = \theta\left[1+\left(\frac{R}{R_d}-1\right)q\right], \tag{2}$$

where R is the gas constant for water vapor, cloud liquid and cloud ice and q is specific humidity. The material (advective) derivative in spherical coordinates is

$$\frac{D}{Dt} = \frac{\partial}{\partial t} + \frac{1}{a\cos^2\phi}\left[U\frac{\partial}{\partial\lambda} + V\cos\phi\frac{\partial}{\partial\phi}\right] + \dot{\eta}\frac{\partial}{\partial\eta}, \tag{3}$$

where a is the radius of the Earth and $\dot{\eta}$ is the η-coordinate vertical velocity ($\dot{\eta} = D\eta/Dt$).

The thermodynamic and moisture equations take on a simple conservative form:

$$\frac{D\theta}{Dt} = 0, \tag{4}$$

$$\frac{Dq}{Dt} = 0. \tag{5}$$

Note that θ is defined here in terms of dry R_d and c_{pd} even in the presence of moisture. This formulation — with dry θ in the thermodynamic equation and θ_v in the pressure gradient term in the momentum equation — is similar to IFS-FVM (Kühnlein et al., 2019), and, the UK Met Office New Dynamics dynamical core. This choice is discussed at length in section 1.5 of Staniforth et al. (2006).

The continuity equation is

$$\frac{\partial}{\partial t}\left(\frac{\partial p}{\partial\eta}\right) + \nabla\cdot\left(\mathbf{v_H}\frac{\partial p}{\partial\eta}\right) + \frac{\partial}{\partial\eta}\left(\dot{\eta}\frac{\partial p}{\partial\eta}\right) = 0, \tag{6}$$

where $\mathbf{v_H} = (u,v)$ is the horizontal wind.

The hydrostatic balance is

$$\frac{\partial\Phi}{\partial\eta} = -R_d\theta_v\left(\frac{p}{p_{oo}}\right)^{\kappa}\frac{\partial\ln p}{\partial\eta}, \tag{7}$$

and the vertical velocity ω is given by

$$\omega = -\int_0^\eta \nabla\cdot\left(\mathbf{v_H}\frac{\partial p}{\partial\eta}\right)d\eta + \mathbf{v_H}\cdot\nabla p = -\int_0^\eta D\frac{dp}{d\eta}d\eta - \int_0^\eta \mathbf{v_H}\cdot\nabla_h\left(\frac{\partial p}{\partial\eta}\right)d\eta + \mathbf{v_H}\cdot\nabla_h p, \tag{8}$$

where $D = \nabla_h\cdot\mathbf{v_H}$ is the divergence.

For semi-implicit (SI) formulation, coupling between the thermodynamic equation and other equations is needed. This, however, is not possible by using (4) alone. Instead, the coupling for the SI system can be achieved by rewriting (4) for Θ'[1], such that

$$\theta(t,\eta,\phi,\lambda) \equiv \Theta'(t,\eta,\phi,\lambda) + \theta_0(p), \tag{9}$$

where $\theta_0(p)$ is a single hydrostatically balanced vertical profile – such as the U.S. standard atmosphere.

[1]Similar formulation is employed in NAVGEM at the Naval Research Laboratory. See Kevin Viner's talk on this: (https://www.newton.ac.uk/files/seminar/20120926120012251-153354.pdf ; https://sms.cam.ac.uk/media/1318288/formats).

We can thus re-write the thermodynamic equation (4) as follows:

$$\frac{D\Theta'}{Dt} + \frac{D\theta_0(p)}{Dt} = \frac{D\Theta'}{Dt} + \omega\frac{\partial\theta_0(p)}{\partial p} = 0, \tag{10}$$

We then linearize (1), (6) and (10) about a dry ($q = 0$) resting basic state:

$$\theta = \theta^R(\eta) + \theta'(t,\eta,\phi,\lambda), \tag{11}$$
$$p_s = p_s^R + p_s'(t,\phi,\lambda), \tag{12}$$
$$p = p^R(\eta) + p'(t,\eta,\phi,\lambda) = A(\eta) + B(\eta)(p_s^R + p_s'(t,\phi,\lambda)), \tag{13}$$

and only retain terms associated with gravity waves. In the above, $\theta^R(\eta) = T^R(p_{oo}/p^R(\eta))^\kappa$ with $T^R = 350$K and $p_s^R = 1000$hPa (as in the IFS-CTRL SI formulation). It is important to note that $\theta^R(\eta) \neq \theta_0(p)$, and hence $\theta'(t,\eta,\phi,\lambda) \neq \Theta'(t,\eta,\phi,\lambda)$. Note also that $p' = B(\eta)p_s'$.

The detailed derivation of the linearized momentum and thermodynamic equations for the SI formulation is given in the Appendix A. In practice, it is further assumed that $\theta_0(p) = \theta_0(p^R)$. For this case the linearized version of the primitive equations to be used in the SI time discretization in the IFS-θ are given below. The momentum equation (1) is formulated for divergence D (i.e., by taking $\nabla_h \cdot$ of (1)). When linearizing about the resting basic state and only retaining linear terms, the momentum equation (1) becomes (Simmons and Burridge, 1981; Simmons and Temperton, 1997):

$$\frac{\partial D}{\partial t} = -\nabla_h^2(\boldsymbol{\gamma}\theta + \boldsymbol{\mu}\ln p_s). \tag{14}$$

Note that the material derivative has become the Eulerian time derivative as the advection term is non-linear. Also note that the Coriolis term is treated as part of the nonlinear term in the IFS. The linearized form of the thermodynamic equation is

$$\frac{\partial\theta}{\partial t} = -\boldsymbol{\tau}D, \tag{15}$$

and the continuity equation (see equation (3) in Simmons and Temperton, 1997)

$$\frac{\partial \ln p_s}{\partial t} = -\boldsymbol{\nu}D. \tag{16}$$

The $\boldsymbol{\gamma}, \boldsymbol{\mu}, \boldsymbol{\tau}, \boldsymbol{\nu}$ operators are defined as follows:

$$\boldsymbol{\gamma}(\theta) = \frac{R_d}{p_{oo}^\kappa}\int_\eta^1 \theta\frac{(p^R)^\kappa}{p^R}m_R^* d\eta, \tag{17}$$

$$\boldsymbol{\mu}(\ln p_s) = \ln p_s R_d T^R, \tag{18}$$

$$\boldsymbol{\tau}(D) = \frac{\partial\theta_0}{\partial p}\int_\eta^0 D\frac{dp^R}{d\eta}d\eta, \tag{19}$$

and

$$\boldsymbol{\nu}(D) = \frac{1}{p_s^R}\int_0^1 D\frac{dp^R}{d\eta}d\eta. \tag{20}$$

Equations (14)-(20) can be combined to give one equation for D only (see also section 2e in Ritchie et al., 1995):

$$\frac{\partial^2 D}{\partial t^2} - \nabla_h^2\boldsymbol{\Gamma}(D) = 0, \tag{21}$$

where

$$\boldsymbol{\Gamma} \equiv \boldsymbol{\gamma}\boldsymbol{\tau} + \boldsymbol{\mu}\boldsymbol{\nu}. \tag{22}$$

The difference from the current operation SI scheme formulated for T is in the $\boldsymbol{\gamma}$ and $\boldsymbol{\tau}$ operators (apart from, of course, the change of variable from T to θ), such that

$$\boldsymbol{\gamma}(\theta) \rightarrow \boldsymbol{\gamma}_{OPER}(T) \equiv R \int_{\eta}^{1} T \frac{d(\ln p^R)}{d\eta} d\eta \tag{23}$$

$$\boldsymbol{\tau} D \rightarrow \boldsymbol{\tau}_{OPER}(D) \equiv \frac{\kappa T^R}{p^R} \int_{0}^{\eta} D \frac{\partial p^R}{d\eta} d\eta, \tag{24}$$

with $\boldsymbol{\nu}$ and $\boldsymbol{\mu}$ staying the same (but only when $\theta_0(p) = \theta_0(p_R)$ as shown in the Appendix A). The description of the discretized SI IFS-θ system is discussed in the Appendix B.

In practice, in IFS-CTRL the advected thermodynamic variable is a smoother quantity $(T - T_b)$, which is essentially independent of underlying orography as T_b depends on surface geopotential height (see section 3.6.3 in ECMWF, 2016). Similarly, the horizontal diffusion is applied on a quantity $(T - T_c)$, where T_c is a function of surface pressure, to avoid a spurious warming over mountain tops. The use of θ as a prognostic variable removes the need for this. Therefore, in IFS-θ the horizontal diffusion is applied on θ directly and no variable dependent on surface geopotential height is subtracted in the advection.

It should be emphasised that in the IFS-θ formulation the semi-Lagrangian advection itself can be performed on either the full θ or Θ', but unless stated otherwise, the results discussed here advect Θ'. It is also possible to advect the natural logarithm of θ because $D\theta/Dt = 0$ is equivalent to $D\ln\theta/Dt = 0$. For realistic θ distributions, taking the natural logarithm of θ substantially reduces its vertical gradient in the advection, potentially reducing discretization errors in the vertical direction arising from the semi-Lagrangian interpolation. As will be shown in section 4, whether Θ' or $\ln\theta$ is advected has an impact on the global mean temperature distribution in the mesosphere, where the vertical gradient in θ is large and vertical resolution poor.

Note that in the simulations with IFS-θ with physical parameterizations (i.e., the 'physics') applied, θ is transformed to T before physics call and then back to θ after the physics has been applied. In other words, physics has not been re-written for θ as a prognostic variable. The physics T tendency is applied as $\dot{Q}/c_{pd}$, where $\dot{Q}$ is the heating rate per unit mass and c_{pd} is dry. To reconcile the inconsistency of using dry θ in the thermodynamic equation and θ_v in the pressure gradient term in the momentum equation, it is suggested in Staniforth et al. (2006) that $\dot{Q}/c_{pd}$ is replaced by $\dot{Q}/(c_{pd}(1+0.84m_v))$, where m_v is the water vapour mixing ratio. However, here we do not apply this correction and use $\dot{Q}/c_{pd}$.

3 Performance under idealized test cases

To test the IFS-θ formulation in an idealized setup, a series of adiabatic test cases are performed: i) dry and moist baroclinic wave; ii) uniform 10 ms^{-1} flow over Schär-type mountain on a small planet; and iii) a falling cold bubble and a rising warm bubble on a small planet. The setup for each test case is described below followed by the comparison of results for IFS-θ to IFS-CTRL. All test cases are performed at TCo79L60 resolution.

3.1 Dry and moist baroclinic instability

The setup for the baroclinic wave test cases is described in detail in Ullrich et al. (2012). The tests are performed on a full size planet (i.e., no small planet setup is used). The model is integrated for 10 days with 1h timestep. The reference potential temperature $\theta_0(p)$ in equation (9) is set to $\theta_0(p) = 350(p_{00}/p_R)^\kappa$.

Figure 1 shows latitude-longitude cross sections of surface pressure (SP) at day 10 for the dry (left column) and moist (right column) baroclinic instability test cases for IFS-CTRL, IFS-θ and the difference between the two. Similarly, Fig. 2 shows height-longitude cross sections of meridional velocity at 60 °N. As can be seen from the figures the agreement between IFS-CTRL and IFS-θ is very good. It should be noted that the differences between IFS-CTRL and IFS-θ in Figs. 1 and 2 are comparable to the differences between the operational spectral transform IFS and the new finite volume dynamical core developed for ECMWF IFS-FVM (see Fig. 3 in Kühnlein et al., 2019, for a slightly different baroclinic instability test case at TCo159L60 resolution). The differences between IFS-CTRL and IFS-θ are observed to decrease for the baroclinic wave test cases with an increase in horizontal resolution (not shown).

3.2 Flow over idealized orography

The Schär-type mountain test case setup is described in detail in Ullrich et al. (2012) (test 2.1). Essentially a uniform 10 m s^{-1} zonal flow in a dry 300 K isothermal non-rotating ($f = 0$) atmosphere is confronted with a 3D Schär-type mountain of height 250 m and centered at the equator, generating a vertically propagating gravity wave. In this test case the radius of the Earth is reduced by a factor of 500 in order to model mesoscale motions at low resolution (Wedi and Smolarkiewicz, 2009). The model is integrated for 30 minutes with 14 s time step size. No Rayleigh friction is applied in this setup and $\theta_0(p)$ in (9) is set to $\theta_0(p) = 350(p_{00}/p_R)^\kappa$.

Figure 3 shows vertical cross sections of temperature perturbation (from in isothermal 300 K reference state) at t=31.5 min for IFS-CTRL and IFS-θ and their differences. Figure 4 shows a horizontal cross section of perturbation temperature at t=31.5 min on model level 50. As can be seen from the figures, the agreement between IFS-CTRL and IFS-θ is again very good with the largest differences occurring near the model top.

3.3 Falling bubble

In this test case an evolution of a large (10 km in the horizontal and 4 km in the vertical) -0.5 K cold bubble and a much smaller (0.6 km in both the horizontal and vertical) +0.15 K warm bubble — prescribed as perturbations to a neutrally stratified environment with θ=300 K— is studied. The setup originally described for two dimensions by Robert (1993) was adopted to three dimensions by Wedi et al. (2009), which is closely followed here. In this test case, the radius of the Earth is reduced by a factor of 200 and the model is integrated for 1250 s with 5 s time step size.

Because of neutral background stratification (i.e., θ is a constant), it was found that advecting potential temperature perturbation from $\theta_0(p) = T_R(p_{00}/p_R)^\kappa$ – with $T_R = 350$ K – resulted in a very large vertical Θ' gradient and an unstable integration. The stability was improved by reducing vertical gradient via a reduction in T_R. However, results closest to the CTRL in terms of the speed of fall of the cold bubble to the surface were achieved by performing semi-Lagrangian advection on the full potential temperature field

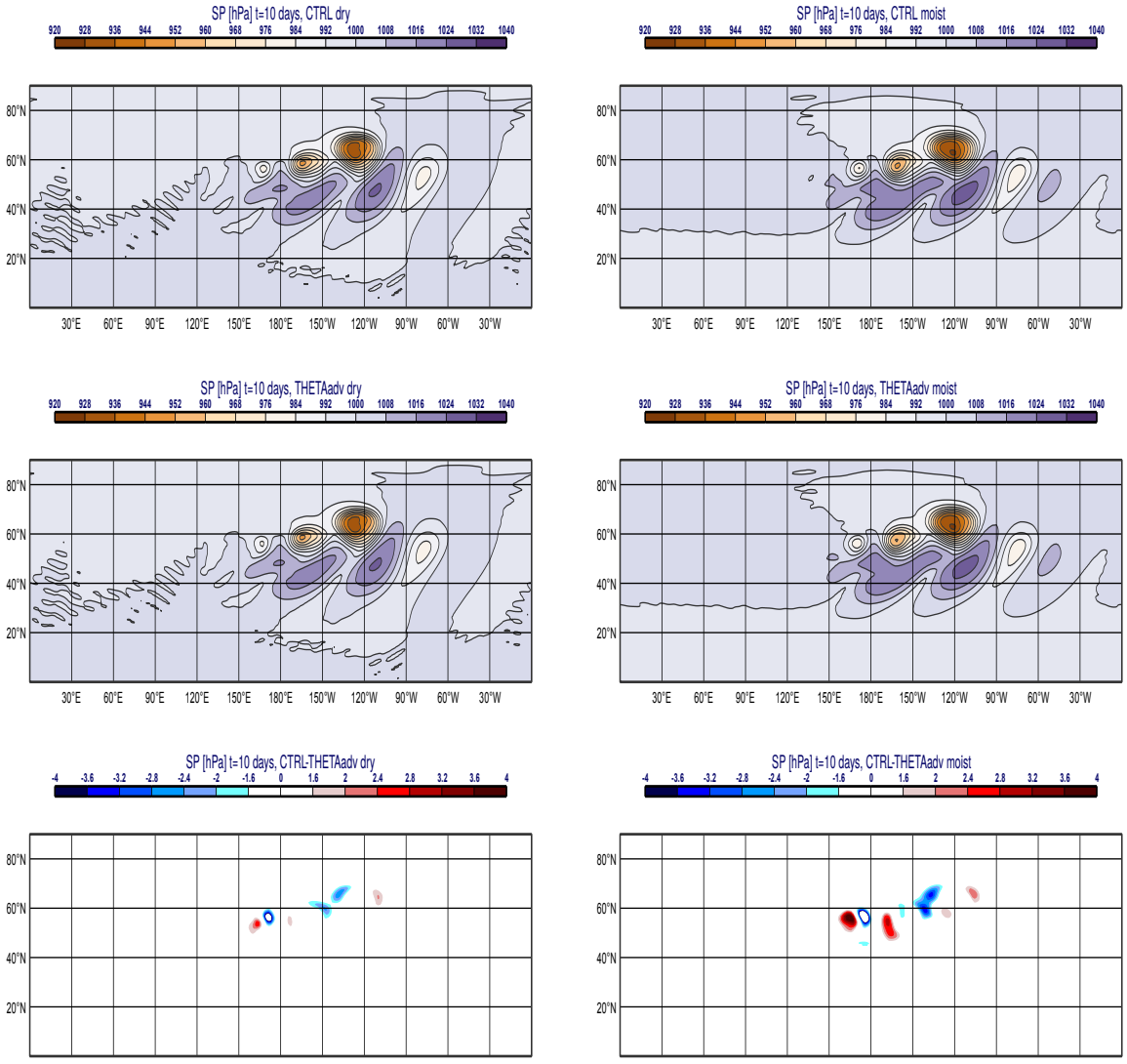

Figure 1: Latitude-longitude cross sections of surface pressure [hPa] at day 10 of (left) dry and (right) moist baroclinic wave test case. Top: IFS-CTRL; middle: IFS-θ; and bottom: IFS-CTRL minus IFS-θ. Resolution is TCo79L60, time step size is 3600s. Note the much smaller contour interval in the bottom panels.

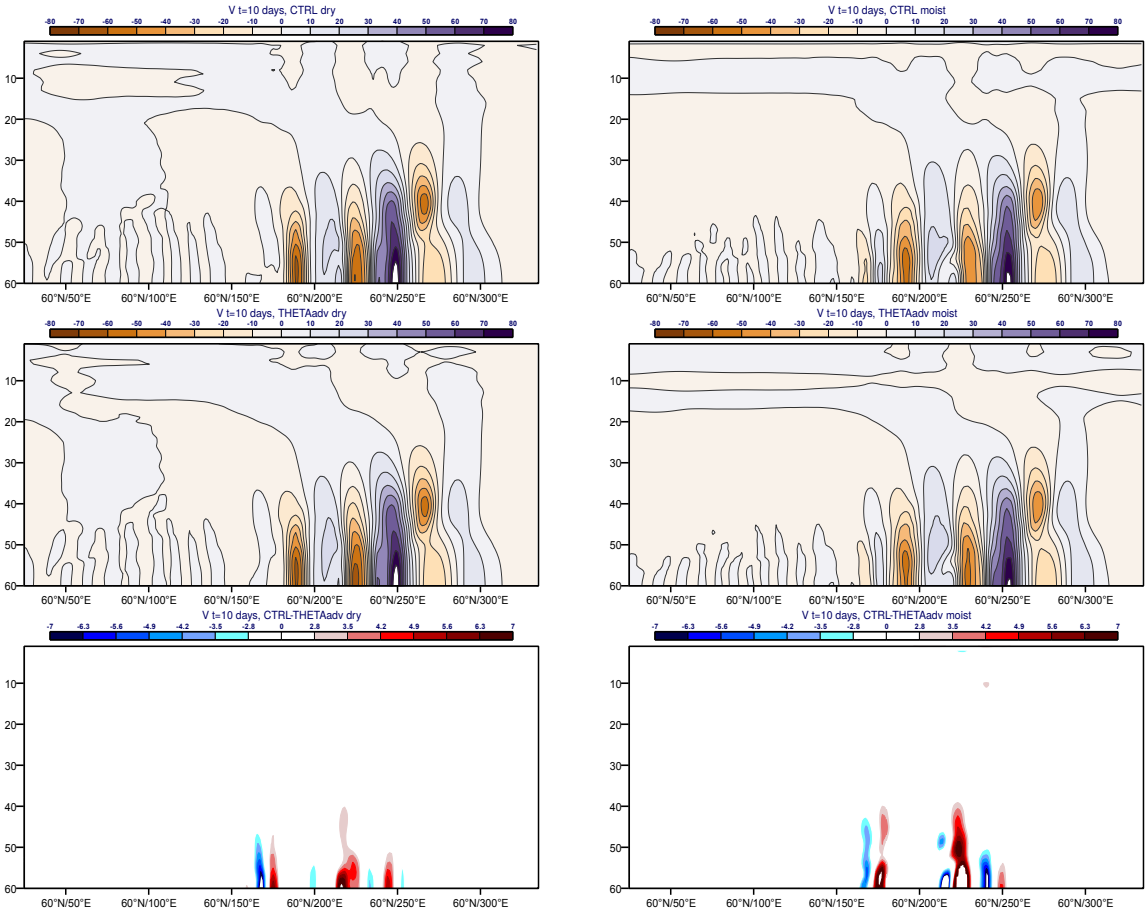

Figure 2: Model level vs. longitude cross sections of meridional velocity [m/s] at 60 °N and t=10 days for (left) dry and (right) moist baroclinic wave test case. Top: IFS-CTRL; middle: IFS-θ; and bottom: IFS-CTRL minus IFS-θ.

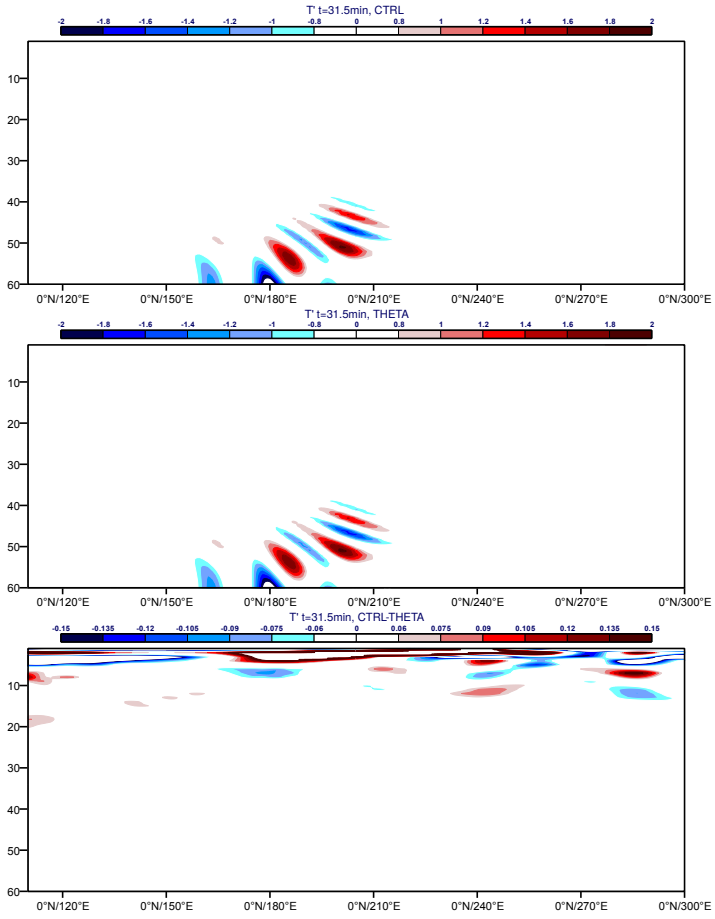

Figure 3: Model level vs. longitude cross sections at the equator of temperature perturbation [K] at t=31.5 min for Schär-type mountain test case. Top: IFS-CTRL; middle: IFS-θ; and bottom: IFS-CTRL minus IFS-θ.

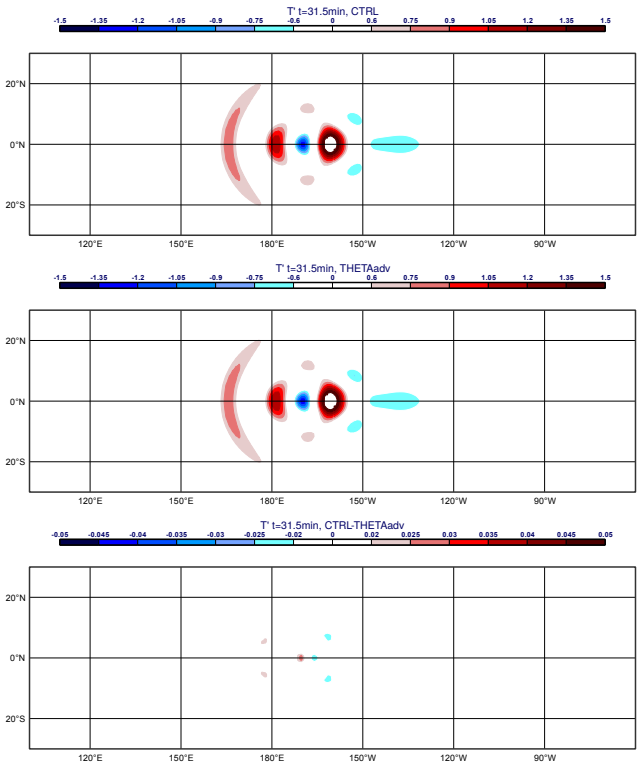

Figure 4: Latitude-longitude cross sections of temperature perturbation [K] on model level 50 at t=31.5 min for Schär-type mountain test case. Top: IFS-CTRL; middle: IFS-θ; and bottom: IFS-CTRL minus IFS-θ.

(i.e., not a difference from $\theta_0(p)$), but still keeping the same semi-implicit formulation using $\theta_0(p) = 350(p_{00}/p_R)^\kappa$. This is likely due to both the largely unchanged stratification during the semi-Lagrangian advection, and, to the largely unchanged semi-implicit formulation.

Figure 5 shows vertical cross sections of potential temperature perturbation from 300 K for IFS-CTRL and IFS-θ for t=0 s, t=250 s, t=500 s and t=1000 s, respectively. The figure shows that the two simulations are very similar up until t=500 s. At later times differences start to emerge, though it is difficult to say which solution is more correct. However, the warming seen in CTRL above 200 hPa, above the falling cold bubble (left column in Fig. 5) appears to be related to the presence of vertical gradient in the advected thermodynamic variable: As semi-Lagrangian advection is performed on the full potential temperature in IFS-θ, the vertical gradient is very small and the warming almost absent. Instead there is a substantial vertical gradient in temperature in IFS-CTRL and the warming is present. The above hypothesis is verified by performing IFS-θ integrations advecting potential temperature perturbation from $\theta_0(p) = T_R(p_{00}/p_R)^\kappa$ with $T_R = 1\ K$, $T_R = 20\ K$, and $T_R = 50\ K$, respectively: It was found that the warming is strongest for $T_R = 50\ K$ (not shown), consistent with $T_R = 50\ K$ producing the largest vertical potential temperature gradient.

4 Performance under full-physics setup

Having assessed the validity of the equations presented in section 2 under idealized setups, it is of interest to establish how IFS-θ performs under more realistic diabatic setup. Firstly, an ensemble of four one-year simulations are performed at TL255L137 resolution to quantify how IFS-θ differs from IFS-CTRL in the zonal mean annual-mean temperature and wind distributions. Subsequently, TCo399L137 (January and July) and TCo1279L137 (January only) resolution medium-range forecasts are performed with IFS-θ and IFS-CTRL to assess if there is any benefit to the skill scores by adopting θ as a prognostic variable. All IFS-θ simulations presented here use $\theta_0(p) = 350(p_{00}/p_R)^\kappa$.

Figure 6 shows pressure vs. latitude cross sections of the annual mean zonal mean zonal wind and temperature differences between IFS-θ and IFS-CTRL. In the troposphere and the stratosphere there is very little impact on the zonal mean circulation as a result of using θ as a prognostic variable, and the small differences seen are likely not robust to sampling variability as only four years are considered. The main difference occurs in the mesosphere, where IFS-θ is 1-2 K warmer than IFS-CTRL. As the mesosphere in IFS is biased warm when compared to Microwave Limb Sounder data (Polichtchouk et al., 2017; Hogan et al., 2017), this warming is undesirable. The warming is likely related to the differences in the vertical gradient between T and θ and ultimately to the different errors in the vertical discretization associated with the two variables (see Polichtchouk et al., 2019). That the vertical θ gradient influences the temperature distribution in the upper stratosphere/mesosphere can be tested by performing the SL advection step for $\ln\theta$. This results in a much shallower vertical gradient for θ in the advection step (as already discussed in section 2). The resulting annual mean zonal mean zonal wind and temperature differences between IFS-$\ln\theta$ and IFS-CTRL are shown in Figure 7, where now the IFS-$\ln\theta$ is colder in the mesosphere than IFS-CTRL.

Next medium-range weather forecast performance of IFS-θ is assessed at TCo399 and TCo1279 horizontal resolutions. Figs. 8-10 show IFS-θ forecast performance against IFS-CTRL when verified against operational analysis for winter and summer season at TCo399L137 resolution. In the troposphere, the impact of using IFS-θ is largely neutral. In the stratosphere, the RMSE of vector winds is marginally improved, and temperature RMSE is degraded in some regions of the upper stratosphere and improved in others. The temperature RMSE change is largely tied to the mean change, as no signal can be seen

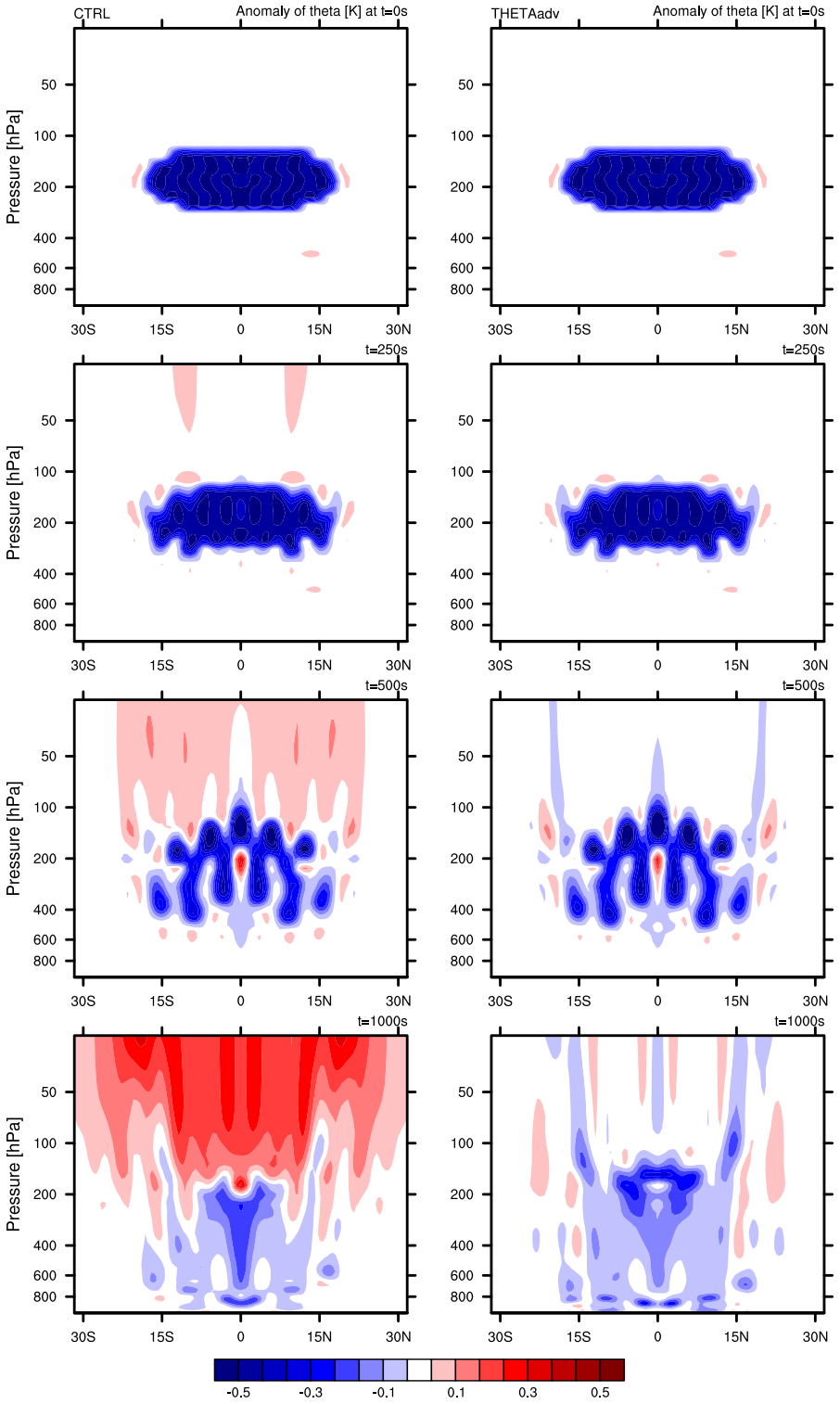

Figure 5: Pressure vs. latitude cross sections of potential temperature perturbation [K] for the bubble test case for (left) IFS-CTRL and (right) IFS-θ at (top row) t=0 s, (second row) t=250 s, (third row) t=500 s, and (bottom row) t=1000 s.

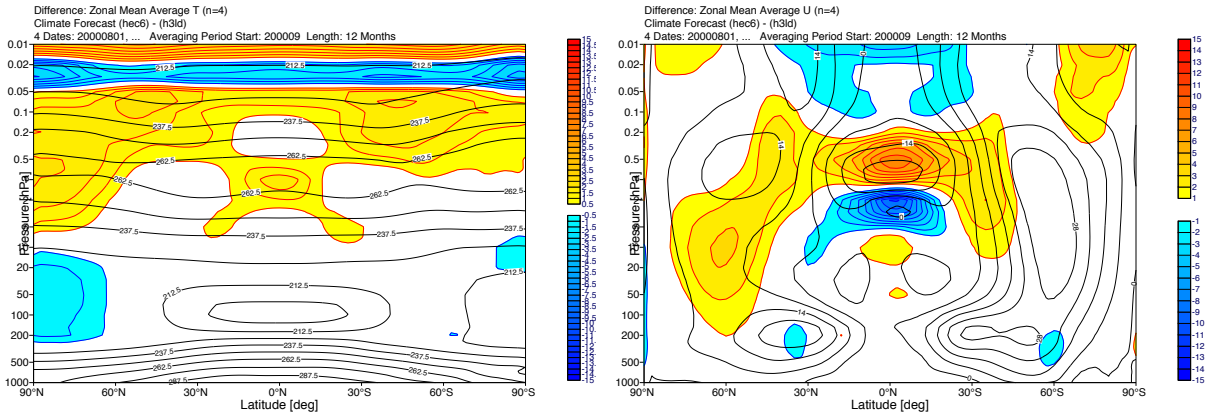

Figure 6: Pressure vs. latitude cross sections of annual mean zonal mean (left) temperature and (right) zonal wind differences between IFS-CTRL and IFS-θ, for four year ensemble of one-year free-running simulations at TL255L137 resolution.

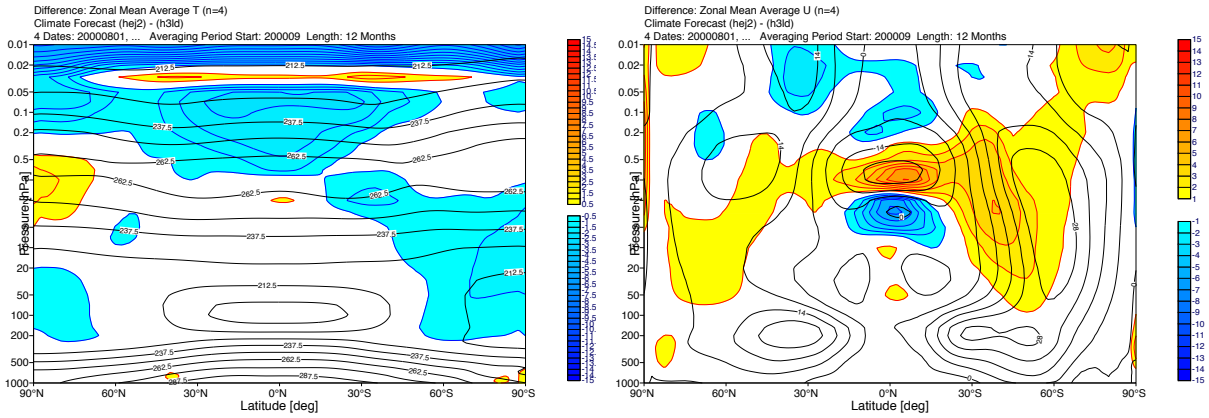

Figure 7: Same as Fig. 6, but for the differences between IFS-CTRL and IFS-$\ln\theta$.

in the temperature anomaly correlation in Fig. 9. As the analysis above 10 hPa is influenced by the underlying model (as comparatively little observations exist to constrain it), whether the small improvements/degradations above 10 hPa are real is not clear.

Figure 11 shows the impact of IFS-θ on medium-range weather forecast performance at TCo1279L137 resolution for July 2017 when verified against operational analysis. It was found that a smaller timestep size of 360 s (instead of 450 s) was necessary for IFS-θ stability. Preliminary investigations into the use of different $\theta_0(p)$ (by choosing $T_R = 250$ K and $T_R = 450$ K, as well as by using a vertically varying T_R), or into advecting $\ln\theta$, did not stabilize the integration with 450 s timestep. Again, the impact of IFS-θ on forecast skill at HRES is similar to TCo399L137 resolution performance with largely neutral impact. Therefore, the conclusion is that IFS-θ performs comparatively to IFS-CTRL.

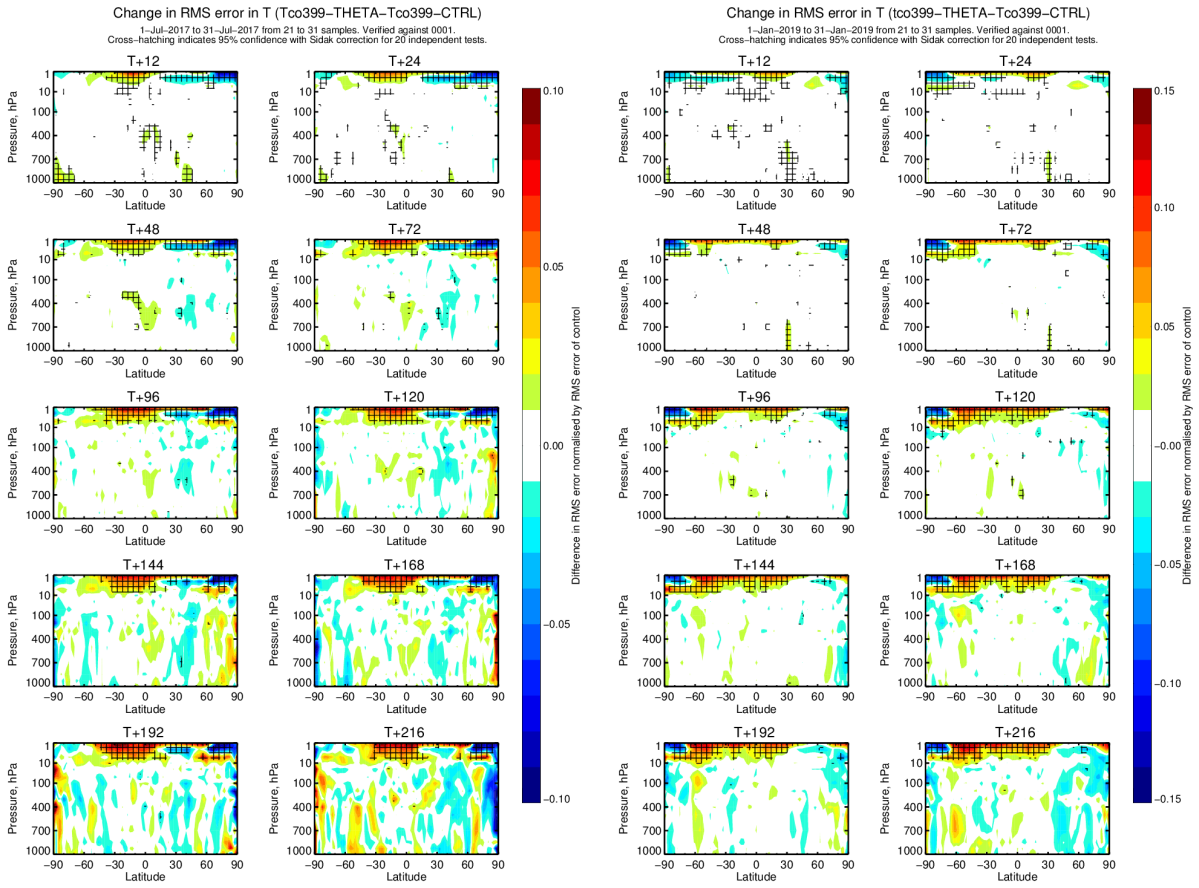

Figure 8: Change in root-mean-square error (RMSE) of temperature forecasts when moving from IFS-CTRL to IFS-θ at TCo399L137 resolution in (left) July 2017 and (right) January 2019 at different forecast validity times. Verification is against operational analysis. Blue (red) colours indicate that errors are smaller (larger) for IFS-θ. Hatched areas indicate statistical significance at an estimated 90% confidence level.

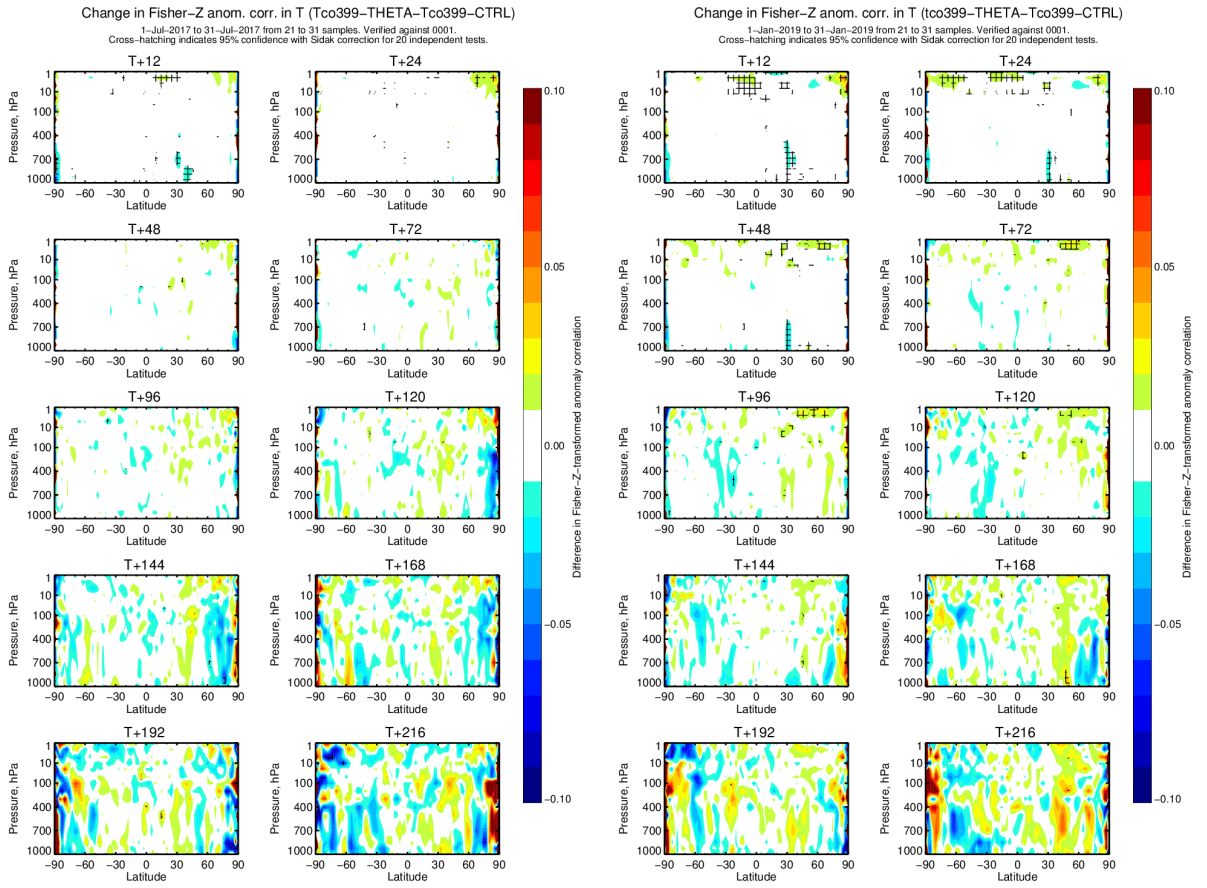

Figure 9: Change in anomaly correlation (AC) of temperature forecasts when moving from IFS-CTRL to IFS-θ at TCo399L137 resolution in (left) July 2017 and (right) January 2019 at different forecast validity times. Verification is against operational analysis. Blue (red) colours indicate that AC is smaller (larger) for IFS-θ, and therefore worse (better) forecast. Hatched areas indicate statistical significance at an estimated 90% confidence level.

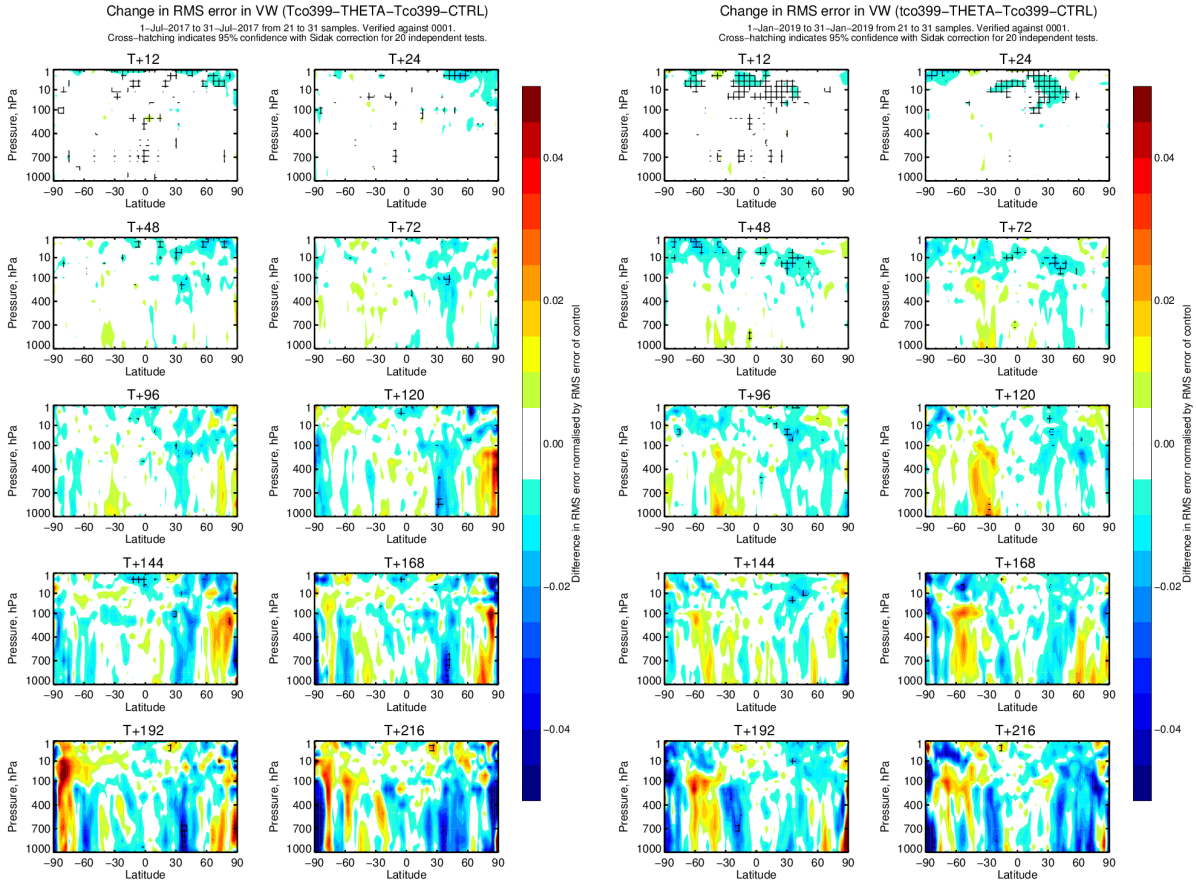

Figure 10: Same as Fig. 8, but for vector winds.

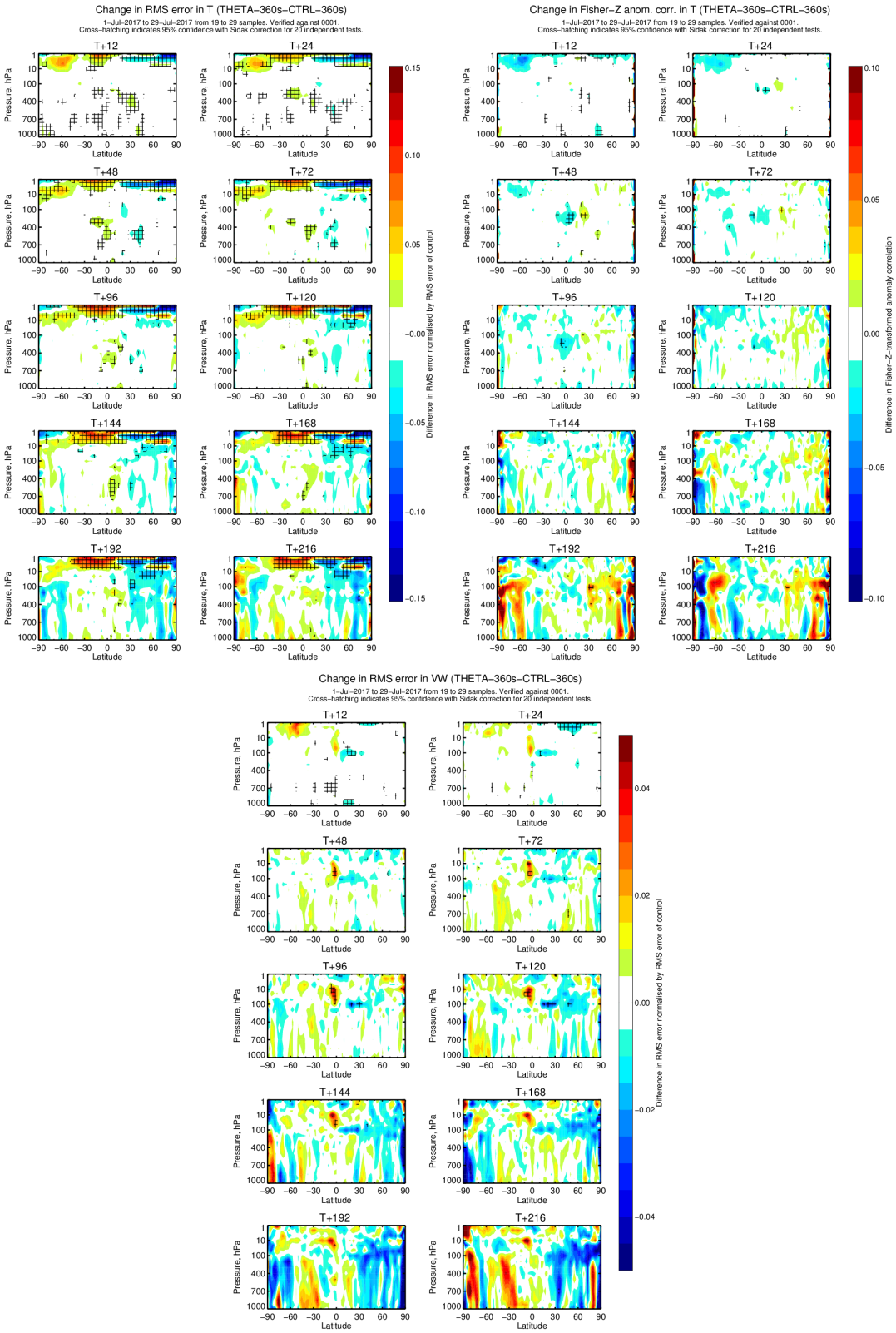

Figure 11: Change in (top left) RMSE and (top right) AC of temperature forecasts and in (bottom) RMSE of vector wind forecasts when moving from IFS-CTRL to IFS-θ at TCo1279L137 resolution in July 2017. Blue (red) colours for RMSE indicate that errors are smaller (larger) for IFS-θ. Blue (red) colours for AC indicate that AC is smaller (larger) for IFS-θ, and therefore worse (better) forecast. Hatched areas indicate statistical significance at an estimated 90% confidence level.

5 Conclusions

In this report, the semi-implicit system using potential temperature as a prognostic variable was derived for hydrostatic primitive equations and implemented into ECMWF IFS (i.e., IFS-θ). It was shown that in the forecast only mode IFS-θ performs similar to the operational version of IFS using temperature as a prognostic thermodynamic variable (i.e., IFS-CTRL) under several scenarios, ranging from idealized adiabatic test cases to full weather forecasts at high resolution. It should be noted that earlier attempts to only perform the semi-Lagrangian advection on θ — leaving the semi-implicit formulation for T unchanged by transforming θ to T at the end of the advection step — resulted in an unstable integration over steep orography.

Interestingly, using θ as a prognostic variable in the advection, is similar to advecting a modified temperature that is essentially independent of underlying orography (see section 3.6.3 in ECMWF, 2016, and section 2 above). Therefore, the use of this modified temperature in IFS-CTRL essentially achieves the benefit that would otherwise be seen from the use of θ as a prognostic variable. Moreover, it should be mentioned that the global enthalpy conservation was not improved in full-physics forecasts by IFS-θ despite much simpler form of the thermodynamic equation. Therefore, the RHS terms in the thermodynamic equation using T as a prognostic variable are not likely a source of enthalpy non-conservation.

Because no apparent benefit is yet seen from using θ as a prognostic variable, it is not recommended that ECMWF pursues this option in its operational forecasts at present. It is of course possible that as the resolution approaches convection-resolving, the benefit of using θ as a prognostic variable becomes more apparent. Moreover, the SI system is only derived here for the hydrostatic primitive equations and tested only in the forecast mode. Whether θ is a better prognostic variable for non-hydrostatic system and/or four dimensional variational data assimilation remains to be assessed.

A Derivation of the hydrostatic SI system using potential temperature as a prognostic variable

The linearization of (1) and (10) about (11-13) is presented here, noting that the discussion follows closely Ritchie et al. (1995) and Wu et al. (2008).

Only the SI terms are discussed below. The dry pressure gradient term is:

$$\nabla_h\Phi + R_d\theta\left(\frac{p}{p_{00}}\right)^\kappa \nabla_h \ln p = \nabla_h\Phi_s - \frac{R_d}{p_{00}^\kappa}\nabla_h\int_1^\eta \theta p^\kappa \frac{\partial \ln p}{\partial\eta}d\eta + R_d\theta\left(\frac{p}{p_{00}}\right)^\kappa \nabla_h \ln p, \tag{25}$$

where we have used

$$\Phi = \Phi_s - \frac{R_d}{p_{00}^\kappa}\int_1^\eta \theta p^\kappa \frac{\partial \ln p}{\partial\eta}d\eta. \tag{26}$$

Now,

$$R_d\theta\left(\frac{p}{p_{00}}\right)^\kappa \nabla_h \ln p = R_d\theta\left(\frac{p}{p_{00}}\right)^\kappa \frac{1}{p}\nabla_h p = R_d\theta\left(\frac{p}{p_{00}}\right)^\kappa \frac{1}{p}\nabla_h(A(\eta)+B(\eta)p_s) =$$
$$R_d\theta\left(\frac{p}{p_{00}}\right)^\kappa \frac{1}{p}B(\eta)\nabla_h p_s = R_d\theta\left(\frac{p}{p_{00}}\right)^\kappa \frac{p_s}{p}B(\eta)\nabla_h \ln p_s, \tag{27}$$

where the last equality comes from multiplying the numerator and the denominator by p_s. Using (27), we can write the pressure gradient term as

$$\nabla_h\Phi + R_d\theta\left(\frac{p}{p_{00}}\right)^\kappa \nabla_h \ln p = \nabla_h\Phi_s - \frac{R_d}{p_{00}^\kappa}\nabla_h\int_1^\eta \theta p^\kappa \frac{\partial \ln p}{\partial\eta}d\eta + R_d\theta\left(\frac{p}{p_{00}}\right)^\kappa \frac{p_s}{p}B(\eta)\nabla_h \ln p_s. \quad (28)$$

Using first (11) and then (9) gives:

$$\nabla_h\theta' = \nabla_h\theta - \nabla_h\theta^R(\eta) = \nabla_h\theta = \nabla_h(\Theta' + \theta_0(p)). \quad (29)$$

When going from p-coordinate to an η-coordinate, the following relationship exists (e.g., Kasahara, 1974)

$$\nabla_\eta A = \nabla_p A + \frac{\partial\eta}{\partial p}(\nabla_\eta p)\left(\frac{\partial A}{\partial\eta}\right), \quad (30)$$

where ∇ denotes any gradient operator (3 or 2-dimensional), the subscript η or p denotes that this coordinate is to be held constant, and A is any scalar function. Applying this relation to $\nabla_h\theta_0(p)$ gives

$$(\nabla_h\theta_0(p))_\eta = (\nabla_h\theta_0(p))_p + \frac{\partial\eta}{\partial p}(\nabla_h p)_\eta\frac{\partial\theta_0(p)}{\partial\eta} = (\nabla_h p)_\eta\frac{\partial\theta_0(p)}{\partial p} =$$
$$(\nabla_h(A(\eta)+B(\eta)p_s))_\eta\frac{\partial\theta_0(p)}{\partial p} = B(\eta)(\nabla_h p_s)_\eta\frac{\partial\theta_0(p)}{\partial p} = B(\eta)p_s(\nabla_h\ln p_s)_\eta\frac{\partial\theta_0(p)}{\partial p}. \quad (31)$$

Dropping the η and p subscripts, and applying (31) to (29) leads to

$$\nabla_h\theta' = \nabla_h(\Theta' + \theta_0(p)) = \frac{\partial\theta_0(p)}{\partial p}B(\eta)p_s\nabla_h\ln p_s + \nabla_h\Theta'. \quad (32)$$

We now linearize the RHS of (28) term by term, using (11)–(13). When linearizing, only terms linear in perturbations are retained. It is also assumed that $\Phi_s = 0$, so that $\nabla_h\Phi_s = 0$ in (28). Let us now focus on the second term on the RHS in (28).

$$-\frac{R_d}{p_{00}^\kappa}\nabla_h\int_1^\eta \theta p^\kappa\frac{\partial\ln p}{\partial\eta}d\eta = -\frac{R_d}{p_{00}^\kappa}\nabla_h\int_1^\eta \theta^R(\eta)p^\kappa\frac{\partial\ln p}{\partial\eta}d\eta - \frac{R_d}{p_{00}^\kappa}\nabla_h\int_1^\eta \theta'(\eta)p^\kappa\frac{\partial\ln p}{\partial\eta}d\eta. \quad (33)$$

Now the second term on the RHS in (33) – when linearizing about p and only keeping terms linear in perturbations – can be written as

$$-\frac{R_d}{p_{00}^\kappa}\nabla_h\int_1^\eta \theta'(\eta)(p^R)^\kappa\frac{\partial\ln p_R}{\partial\eta}d\eta = -\frac{R_d}{p_{oo}^\kappa}\int_1^\eta(\nabla_h\theta')\frac{(p^R)^\kappa}{p^R}m_R^*d\eta, \quad (34)$$

where $m_R^* \equiv \frac{\partial p^R}{\partial\eta} = \frac{\partial A}{\partial\eta} + p_s^R\frac{\partial B}{\partial\eta}$. We can now substitute (32) into (34) to give:

$$-\frac{R_d}{p_{oo}^\kappa}\int_1^\eta(\nabla_h\theta')\frac{(p^R)^\kappa}{p^R}m_R^*d\eta = -\frac{R_d}{p_{oo}^\kappa}\int_1^\eta\left(\frac{\partial\theta_0(p)}{\partial p}B(\eta)p_s\nabla_h\ln p_s + \nabla_h\Theta'\right)\frac{(p^R)^\kappa}{p^R}m_R^*d\eta, \quad (35)$$

so that

$$-\frac{R_d}{p_{00}^\kappa}\nabla_h\int_1^\eta \theta'(\eta)(p^R)^\kappa\frac{\partial\ln p_R}{\partial\eta}d\eta = -\frac{R_d}{p_{oo}^\kappa}\int_1^\eta\left(\frac{\partial\theta_0(p)}{\partial p}B(\eta)p_s\nabla_h\ln p_s + \nabla_h\Theta'\right)\frac{(p^R)^\kappa}{p^R}m_R^*d\eta. \quad (36)$$

Lets now focus on the first term on the RHS of (33). Retaining only the linear terms, it can be written as:

$$-\frac{R_d}{p_{00}^{\kappa}}\nabla_h\int_1^{\eta}\theta^R(\eta)p^{\kappa}\frac{\partial \ln p}{\partial \eta}d\eta=-\frac{R_d}{p_{00}^{\kappa}}\nabla_h\int_1^{\eta}\theta^R(\eta)(p^R)^{\kappa}\frac{\partial \ln p}{\partial \eta}d\eta=-R_dT^R\nabla_h\int_1^{\eta}\frac{\partial \ln p}{\partial \eta}d\eta$$
$$=-R_dT^R\nabla_h\int_{p_s}^{p(\eta)}d\ln p=-R_dT^R\nabla_h\ln p+R_dT^R\nabla_h\ln p_s. \quad (37)$$

The last term in (37) can be further linearized as

$$-R_dT^R\nabla_h\ln p+R_dT^R\nabla_h\ln p_s=-\frac{R_dT^R}{p^R}\nabla_h p^{'}+R_dT^R\nabla_h\ln p_s=$$
$$-\frac{R_dT^RB(\eta)}{p^R}\nabla_h p_s^{'}+R_dT^R\nabla_h\ln p_s. \quad (38)$$

Combining (36) and (38) finally gives the linearized version of the second term on the RHS of (28):

$$-\frac{R_d}{p_{oo}^{\kappa}}\nabla_h\int_1^{\eta}\theta p^{\kappa}\frac{\partial \ln p}{\partial \eta}d\eta\approx$$
$$-\frac{R_dT^RB(\eta)}{p^R}\nabla_h p_s^{'}+R_dT^R\nabla_h\ln p_s-\frac{R_d}{p_{oo}^{\kappa}}\int_1^{\eta}\left(\frac{\partial\theta_0(p)}{\partial p}B(\eta)p_s\nabla_h\ln p_s+\nabla_h\Theta^{'}\right)\frac{(p^R)^{\kappa}}{p^R}m_R^*d\eta. \quad (39)$$

The third term on the RHS of (28) is yet be linearized to obtain a linearized version of the pressure gradient term. It can be linearized as follows:

$$R_d\theta\left(\frac{p}{p_{00}}\right)^{\kappa}\frac{p_s}{p}B(\eta)\nabla_h\ln p_s\approx R_d\theta^R\left(\frac{p^R}{p_{00}}\right)^{\kappa}\frac{1}{p^R}B(\eta)\nabla_h p_s^{'}=\frac{R_dT_RB(\eta)}{p^R}\nabla_h p_s^{'}. \quad (40)$$

Therefore this term cancels with the first term on the RHS of (39). Finally, the linearized pressure gradient term (28) reads as:

$$\nabla_h\Phi^{'}+R_d\Theta^{'}\left(\frac{p}{p_{00}}\right)^{\kappa}\nabla_h\ln p=R_dT^R\nabla_h\ln p_s-\frac{R_d}{p_{oo}^{\kappa}}\int_1^{\eta}\left(\frac{\partial\theta_0(p)}{\partial p}B(\eta)p_s^R\nabla_h\ln p_s+\nabla_h\Theta^{'}\right)\frac{(p^R)^{\kappa}}{p^R}m_R^*d\eta \quad (41)$$

We now need to linearize the vertical advection of $\frac{\partial\theta_0}{\partial p}$ term in (10). For this we need to linearize (8) first about a resting basic state. This means that the two terms on the RHS of (8) dissappear (as we ignore quadratic terms in perturbation) and we are left with the following (see Appendix in Wu et al. (2008) for details):

$$-\omega\frac{\partial\theta_0}{\partial p}\approx\frac{\partial\theta_0}{\partial p}\int_0^{\eta}D\frac{dp^R}{d\eta}d\eta. \quad (42)$$

Therefore, by using (41) and (42) the linearized version of the primitive equations to be used in the SI time discretization can now be written down:

$$\frac{\partial D}{\partial t}=-\nabla_h^2(\boldsymbol{\gamma}\Theta'+\boldsymbol{\mu}\ln p_s), \quad (43)$$

$$\frac{\partial\Theta'}{\partial t}=-\boldsymbol{\tau}D, \quad (44)$$

$$\frac{\partial\ln p_s}{\partial t}=-\boldsymbol{\nu}D. \quad (45)$$

The $\boldsymbol{\gamma}, \boldsymbol{\mu}, \boldsymbol{\tau}, \boldsymbol{\nu}$ operators are defined as follows:

$$\boldsymbol{\gamma}(\Theta') = \frac{R_d}{p_{oo}^{\kappa}} \int_{\eta}^{1} \Theta' \frac{(p^R)^{\kappa}}{p^R} m_R^* d\eta, \tag{46}$$

$$\boldsymbol{\mu}(\ln p_s) = \ln p_s \left(R_d T^R + \frac{R_d p_s^R}{p_{oo}^{\kappa}} \int_{\eta}^{1} \frac{\partial \theta_0(p^R)}{\partial p} B(\eta) \frac{(p^R)^{\kappa}}{p^R} m_R^* d\eta \right), \tag{47}$$

$$\boldsymbol{\tau}(D) = \frac{\partial \theta_0}{\partial p} \int_{\eta}^{0} D \frac{dp^R}{d\eta} d\eta, \tag{48}$$

and

$$\boldsymbol{\nu}(D) = \frac{1}{p_s^R} \int_{0}^{1} D \frac{dp^R}{d\eta} d\eta. \tag{49}$$

Note that the SI form of the continuity equation has not changed from its original implementation in IFS using T as a prognostic thermodynamic variable.

As in section 2, (43)-(49) can be combined to give one equation for D only:

$$\frac{\partial^2 D}{\partial t^2} - \nabla_h^2 \boldsymbol{\Gamma}(D) = 0, \tag{50}$$

where

$$\boldsymbol{\Gamma} \equiv \boldsymbol{\gamma}\boldsymbol{\tau} + \boldsymbol{\mu}\boldsymbol{\nu}. \tag{51}$$

Or in the spherical harmonic notation, (50) reads as:

$$\frac{\partial^2 D_n^m}{\partial t^2} + \frac{n(n+1)}{a^2} \boldsymbol{\Gamma}(D) = 0, \tag{52}$$

where (n,m) are the total and zonal wavenumbers in the spherical harmonic expansion.

In practice, $\theta_0(p)$ in (9) is taken to be $\theta_0(p_R)$, where p_R does not depend on the horizontal direction. Therefore (31) reduces to zero and (32) is simply:

$$\nabla_h \theta' = \nabla_h \theta = \nabla_h \Theta'. \tag{53}$$

Therefore the term proportional to $B(\eta)$ in (41) disappears and (47) reduces to (18), which is the same as in the operational implementation for T as a prognostic variable. Given (53) and that $\partial\Theta'/\partial t = \partial\theta/\partial t$, the linearized equations (43) and (44) can be written in terms of θ. This leads to the formulation presented in section 2.

B The discretized SI system

The discretized two-time level SISL system of equations can be written for any prognostic variable X as:

$$X_A^{t+\Delta t} = X_D^t + \Delta t \mathscr{R}_M^{t+0.5\Delta t} + \Delta t \{ -\beta \mathscr{L}_M^{t+0.5\Delta t} + 0.5\beta \mathscr{L}_D^t + 0.5\beta \mathscr{L}_A^{t+\Delta t} \}, \tag{54}$$

where the curly bracketed terms in (54) include the SI correction of linearised terms $\mathscr{L}$, and, β is the semi-implicitness factor, such that $\beta = 1$ corresponds to a semi-implicit time integration and $\beta = 0$ to an explicit time integration, respectively. $\mathscr{R}$ denotes all terms in the prognostic equations other than the

material derivative DX/Dt; A is the arrival point and D is the departure point; the mid-point M of a quantity $\mathcal{N}$ is estimated by the extrapolating scheme SETTLS (Hortal, 2002):

$$\mathcal{N}_M^{t+0.5\Delta t} \simeq 0.5(\mathcal{N}_D^t + \tilde{\mathcal{N}}_A^{t+\Delta t})$$

where $\tilde{\mathcal{N}}_A^{t+\Delta t}$ is the extrapolated guess

$$\tilde{\mathcal{N}}_A^{t+\Delta t} = \mathcal{N}_D^t + \frac{\mathcal{N}_A^t - \mathcal{N}_D^{t-\Delta t}}{\Delta t}\Delta t.$$

Equivalently, equation (54) can be written as

$$X_A^{t+\Delta t} = X^* + 0.5\beta\mathcal{L}_A^{t+\Delta t} \tag{55}$$

where X^* represents the first four terms on the RHS of equation (54).

The solution procedure in the spectral space is then as follows:

$$\tilde{\theta}^{t+\Delta t} = \tilde{\theta}^* - 0.5\beta\Delta t\boldsymbol{\tau}\tilde{D}^{t+\Delta t}, \tag{56}$$

$$\ln \tilde{p_s}^{t+\Delta t} = \tilde{\mathcal{P}}^* - 0.5\beta\Delta t\boldsymbol{\nu}\tilde{D}^{t+\Delta t}, \tag{57}$$

$$\tilde{D}^{t+\Delta t} = \tilde{\mathcal{D}}^* - 0.5\beta\Delta t\nabla^2(\boldsymbol{\gamma}\tilde{\theta}^{t+\Delta t} + \boldsymbol{\mu}\ln \tilde{p_s}^{t+\Delta t}), \tag{58}$$

where $\tilde{X}^*$ is the spectral representations of X^*. This leads to the following structure equation:

$$\{1 - (0.5\beta\Delta t)^2(\boldsymbol{\gamma}\boldsymbol{\tau} + \boldsymbol{\nu}\boldsymbol{\mu})\nabla^2\}\tilde{D}^{t+\Delta t} = \tilde{\mathcal{D}}^{**} \tag{59}$$

where

$$\tilde{\mathcal{D}}^{**} = \tilde{\mathcal{D}}^* - (0.5\beta\Delta t)\nabla^2(\boldsymbol{\gamma}\tilde{\theta}^* + \boldsymbol{\mu}\tilde{\mathcal{P}}^*). \tag{60}$$

Therefore implementing the SI procedure in IFS for θ as a prognostic variable involves modification of the pre-computed matrices $\{\boldsymbol{\gamma}, \boldsymbol{\tau}\}$. The success of the above formulation assumes that $(\boldsymbol{\gamma}\boldsymbol{\tau} + \boldsymbol{\nu}\boldsymbol{\mu})$ can be inverted.

References

ECMWF (2016). IFS documentation. CY46R1. part iii: Dynamics and numerical procedures. *http://www.ecmwf.int/en/forecasts/documentation-and-support/changes-ecmwf-model/ifs-documentation.*.

Hogan, R. J., M. Ahlgrimm, G. Balsamo, A. Beljaars, P. Berrisford, A. Bozzo, F. Di Giuseppe, R. M. Forbes, T. Haiden, S. Lang, et al. (2017). *Radiation in numerical weather prediction*. European Centre for Medium-Range Weather Forecasts.

Hogan, T. F., M. Liu, J. A. Ridout, M. S. Peng, T. R. Whitcomb, B. C. Ruston, C. A. Reynolds, S. D. Eckermann, J. R. Moskaitis, N. L. Baker, et al. (2014). The navy global environmental model. *Oceanography 27*(3), 116–125.

Hortal, M. (2002). The development and testing of a new two-time-level semi-Lagrangian scheme (SETTLS) in the ECMWF forecast model. *Quarterly Journal of the Royal Meteorological Society 128*(583), 1671–1687.

Kasahara, A. (1974). Various Vertical Coordinate Systems Used for Numerical Weather Prediction. *Monthly Weather Review 102*(7), 509–522.

Kühnlein, C., W. Deconinck, R. Klein, S. Malardel, Z. P. Piotrowski, P. K. Smolarkiewicz, J. Szmelter, and N. P. Wedi (2019). FVM 1.0: a nonhydrostatic finite-volume dynamical core for the IFS. *Geoscientific Model Development 12*(2), 651–676.

Polichtchouk, I., R. J. Hogan, T. G. Shepherd, P. Bechtold, T. Stockdale, S. Malardel, S.-J. Lock, and L. Magnusson (2017). *What influences the middle atmosphere circulation in the IFS?* European Centre for Medium Range Weather Forecasts.

Polichtchouk, I., T. Stockdale, P. Bechtold, M. Diamantakis, S. Malardel, I. Sandu, F. Vána, and N. Wedi (2019, 06). Control on stratospheric temperature in IFS: resolution and vertical advection. (847).

Ritchie, H., C. Temperton, A. Simmons, M. Hortal, T. Davies, D. Dent, and M. Hamrud (1995). Implementation of the semi-Lagrangian method in a high-resolution version of the ECMWF forecast model. *Monthly Weather Review 123*(2), 489–514.

Robert, A. (1993). Bubble Convection Experiments with a Semi-implicit Formulation of the Euler Equations. *Journal of the Atmospheric Sciences 50*(13), 1865–1873.

Simmons, A. J. and D. M. Burridge (1981). An energy and angular-momentum conserving vertical finite-difference scheme and hybrid vertical coordinates. *Monthly Weather Review 109*(4), 758–766.

Simmons, A. J. and C. Temperton (1997). Stability of a two-time-level semi-implicit integration scheme for gravity wave motion. *Monthly weather review 125*(4), 600–615.

Staniforth, A., A. White, N. Wood, J. Thuburn, M. Zerroukat, E. Cordero, T. Davies, and M. Diamantakis (2006). Joy of UM 6.3 model formulation. *Unified Model documentation paper 15*.

Ullrich, P. A., C. Jablonowski, J. Kent, P. H. Lauritzen, R. D. Nair, and M. A. Taylor (2012). Dynamical core model intercomparison project (DCMIP) test case document. *DCMIP Summer School 83*.

Wedi, N., K. Yessad, and A. Untch (2009, 10). The non-hydrostatic global IFS/ARPEGE model: model formulation and testing. (594), 34.

Wedi, N. P. and P. K. Smolarkiewicz (2009). A framework for testing global non-hydrostatic models. *Quarterly Journal of the Royal Meteorological Society 135*(639), 469–484.

Wood, N., A. Staniforth, A. White, T. Allen, M. Diamantakis, M. Gross, T. Melvin, C. Smith, S. Vosper, M. Zerroukat, and J. Thuburn (2014). An inherently mass-conserving semi-implicit semi-lagrangian discretization of the deep-atmosphere global non-hydrostatic equations. *Quarterly Journal of the Royal Meteorological Society 140*(682), 1505–1520.

Wu, T., R. Yu, and F. Zhang (2008). A modified dynamic framework for the atmospheric spectral model and its application. *Journal of the Atmospheric Sciences 65*(7), 2235–2253.